PROCEEDINGS OF SCIENCE

Shift of UHECR source images by the intergalactic magnetic field

Alexander Korochkin,[a] **Konstantin Dolgikh,**[b,c] **Grigory Rubtsov,**[b] **Dmitri Semikoz**[d] **and Igor Tkachev**[b,e]

[a] *Université Libre de Bruxelles, CP225 Boulevard du Triomphe, 1050 Brussels, Belgium*
[b] *Institute for Nuclear Research of the Russian Academy of Sciences, Moscow 117312, Russia*
[c] *Lomonosov Moscow State University, Faculty of Physics, Moscow 119991, Russia*
[d] *Université Paris Cité, CNRS, Astroparticule et Cosmologie, 75006 Paris, France*
[e] *Novosibirsk State University, Novosibirsk 630090, Russia*

We study the propagation of ultra-high-energy cosmic rays (UHECRs) in the local intergalactic magnetic field (IGMF) within a radius of <10 Mpc around the Milky Way. Assuming that the field strength is in the range of 1–3 nG and the correlation length is between 0.01 and 1 Mpc, we demonstrate that the IGMF can not only blur the source image but also shift its position, mimicking the effect of the coherent Galactic magnetic field (GMF). This introduces additional uncertainty in identifying UHECR sources due to the displacement of the source image in the IGMF. Unlike the image shift caused by the coherent GMF, which is determined by its global structure, the shift in the IGMF depends on the specific realization of the turbulent magnetic field between the source and the observer which is much more difficult to control. Finally, we apply this effect to potential sources of the UHECR excess in the Cen A region.

39th International Cosmic Ray Conference (ICRC2025)
15–24 July 2025
Geneva, Switzerland

PoS(ICRC2025)307

1. Introduction

At energies above $E > 10^{19}$ eV, the mass composition of UHECRs is dominated by intermediate-mass nuclei [?], which are expected to undergo significant deflections in the Galactic magnetic field (GMF). This is supported by recent coherent GMF models, such as `UF23`[1] and `KST24`[2], which predict strong deflections across large portions of the sky. In addition to the GMF, UHECR propagation can also be influenced by strong IGMF, with the strength of B$\sim 0.1 - 1$ G [3]. The IGMF in the local Universe could be even stronger if the Milky Way resides within a filament of the large-scale structure (LSS) or if local fields have been enhanced by feedback from nearby galaxy groups, such as the Council of Giants [4].

The simplest and computationally efficient way to account for this effect is the smearing angle approximation. In this approximation, the initial point-like image of the source is replaced by a symmetric halo with angular size δ. The size δ, in turn, depends on the IGMF strength B, the correlation length L_c, and the distance to the source D such that $\delta \propto B\sqrt{DL_c}/E$. At the same time, the position of the center of the source's image remains unchanged and points to the direction to the source.

The isotropic smearing approximation is valid when $D \gg L_c$. In contrast, when $D \ll L_c$, the propagation of UHECRs is ballistic, and the source image remains nearly point-like for a fixed energy. There exists an intermediate regime characterized by $L_c \approx (0.001 - 1) \times D$ and $R_L > L_c$, where R_L is the particles' Larmor radius. We will refer to this as the focusing regime.

In what follows, we study the appearance of the source images in the focusing regime, logically building upon our previous findings [5, 6]. We show that in this regime the IGMF not only smears the source image but also shifts its position thus mimicking the effect of the coherent GMF. This complicates the search for UHECR sources by introducing additional uncertainty related to the shift of the source image in the IGMF. Unlike the image shift in the coherent GMF, which is determined by its global configuration, the shift in the IGMF depends on a specific realization of the turbulent field between the source and the observer, and thus is much more difficult to control.

2. UHECR source images in the focusing regime

To construct images of UHECR sources as they would appear after propagation through the IGMF, we performed a series of numerical simulations. For 3D modeling of UHECR propagation we used the publicly available Monte Carlo code `CRbeam` [1][7]. The IGMF was assumed to be spatially uniform with a Kolmogorov spectrum $P_B(k)$ over a wavelength range from L_{max} down to $L_{min} = L_{max}/100$:

$$P_B(k) = \begin{cases} 0 & k < k_{min} \\ A\left(\frac{k_{min}}{k}\right)^m & k_{min} \le k \le k_{max} \\ 0 & k_{max} < k \end{cases} \quad (1)$$

where $k_{min} = 2\pi/L_{max}$, $k_{max} = 2\pi/L_{min}$ and A is the normalization constant, determined by the condition that the root-mean-square (rms) value of the magnetic field equals B. The exponent was fixed to $m = 11/3$, as for Kolmogorov turbulence.

[1] https://github.com/okolo/mcray

For consistency with previous studies, we present our results in terms of the IGMF correlation length L_c . We define L_c following [8] as

$$L_c = \frac{1}{2} L_{\max} \frac{n-1}{n} \frac{1-(L_{\min}/L_{\max})^n}{1-(L_{\min}/L_{\max})^{n-1}}. \tag{2}$$

In the case of Kolmogorov turbulence considered in this paper, where $n = 5/3$ this yields $L_c \approx L_{\max}/5$ for $L_{\min} \ll L_{\max}$.

We assumed that the source emits UHECRs uniformly within a cone of a given opening angle and axis direction, pointing toward the observer. The opening angle was chosen to be sufficiently large to ensure that the results are independent of its specific value. UHECR energy losses were neglected since in all simulations the distance between the source and the observer does not exceed $D = 10$ Mpc. The rigidity was fixed to $R = 10$ EV. We consider only steady-state sources, assuming that the source duty cycle is much longer than the UHECR time delay in the IGMF and GMF. Each simulation stops when $N = 1000$ particles hit the spherical observer whose radius was set to $R_{\rm obs} = 100$ kpc. The value of N was chosen to ensure sufficient event statistics.

Given the set of detected events emitted with the initial momenta $\mathbf{p}_{i0}$, the image of the source at the observer is determined by their final momenta, $\mathbf{p}_i$, where the index i labels individual particles. For subsequent calculations, it is useful to introduce dimensionless unit vectors representing the momentum directions, $\mathbf{n}_{i0} = \mathbf{p}_{i0}/p_{i0}$ and $\mathbf{n}_i = \mathbf{p}_i/p_i$, and a unit vector $\mathbf{s}$ pointing from the source to the observer. The mean final direction of the particles, $\mathbf{n}_{\rm avg}$, is then given by

$$\mathbf{n}_{\rm avg} = \frac{\langle \mathbf{n}_i \rangle}{|\langle \mathbf{n}_i \rangle|}, \tag{3}$$

where the angle brackets denote averaging over the set of events $\langle \mathbf{n}_i \rangle = \frac{1}{N} \sum_{i=1}^{N} \mathbf{n}_i$. The deflection angle α_i of a particle is defined as

$$\cos \alpha_i = \mathbf{n}_i \cdot \mathbf{n}_{i0}, \tag{4}$$

while the angle δ_i between a particle's final direction and the mean final direction is given by

$$\cos \delta_i = \mathbf{n}_i \cdot \mathbf{n}_{\rm avg}. \tag{5}$$

Averaging over the set of detected particles, we arrive at the following three angles

$$\begin{cases} \alpha = \alpha_{\rm rms} = \sqrt{\langle \alpha_i^2 \rangle} \\ \delta = \delta_{\rm rms} = \sqrt{\langle \delta_i^2 \rangle} \\ \theta = \arccos(\mathbf{n}_{\rm avg} \cdot \mathbf{s}) \end{cases} \tag{6}$$

each with a clear physical meaning. The angle α corresponds to the RMS deflection angle of the particle from its initial direction, δ represents the angular size of the source's image as seen by the observer, and θ corresponds to the average shift of the entire image from the true direction to the source. Below we numerically compute these angles using Eq. (6) for the different configurations of the magnetic field.

2.1 Approximation of uncorrelated trajectories

We begin with the simplest case of uncorrelated trajectories. In this approximation, each UHECR trajectory is treated as completely independent of the others. For particles emitted by a point source, this approximation is not entirely realistic, as particles that are initially closely aligned propagate through nearly the same magnetic field at short distances from the source. However, it becomes valid at large distances from the source, where the particles lose memory of their initial conditions. Moreover, in this approximation, the angles α, δ, and θ can be computed analytically.

The classical analytical results for the case of uncorrelated trajectories can be found for example in [9]. Reproducing them for the magnetic field spectrum described above and assuming that the propagation distance is much greater than the maximum scale of the IGMF $D \gg L_{\rm max}$, we obtain

$$\begin{cases} \alpha = 3.74^\circ \cdot Z \left[\frac{B}{1\,\mathrm{nG}}\right] \left[\frac{E}{10^{19}\,\mathrm{eV}}\right]^{-1} \left[\frac{D}{10\,\mathrm{Mpc}}\right]^{\frac{1}{2}} \left[\frac{L_{\rm max}}{500\,\mathrm{kpc}}\right]^{\frac{1}{2}} \\ \delta = \alpha/\sqrt{3} \\ \theta = 0. \end{cases} \tag{7}$$

Note that while the expression for α depends on assumed magnetic field spectrum, the relation between the image size δ and α is general and holds for any magnetic field, in the regime $D \gg L_{\rm max}$. The absence of image shift ($\theta = 0$) is also a general result and follows from the presence of axial symmetry.

2.2 Shift of source images in the turbulent IGMF

In this section, we repeat the simulation from the previous section, with the only difference that all particles are now propagated through the same realization of the magnetic field. As we show below, this leads to a non-zero angle θ defined in Eq. (6), resulting in a shift of the entire source image. On the other hand, this introduces a dependence of the results on the specific positions of the source and the observer within a given IGMF realization. To investigate this effect, we perform 30 simulations, each with its own realization of the IGMF.

The results of the simulations for a source at a distance of $D = 4$ Mpc are shown in Figs. 1 and 2. Fig. 1 shows the dependence of the image size δ on the IGMF correlation length $L_{\rm c}$. The size of the image approaches the theoretical prediction for uncorrelated trajectories, given by Eq. (7), only for small correlation lengths, $L_{\rm c} \lesssim 0.1$ Mpc. This regime corresponds to the propagation of particles through approximately $D/L_{\rm c} \gtrsim 100$ magnetic domains. In contrast, for larger correlation lengths ($L_{\rm c} > 0.1$ Mpc), the image size remains small and even decreases with increasing $L_{\rm c}$.

On the other hand, as seen in Fig. 1, there is a non-zero shift of the entire source image. At small correlation lengths, the shift tends to zero, but increases rapidly as $L_{\rm c}$ grows. Notably, when the correlation length is in the range $\sim 0.1\text{˜}1$ Mpc, the image shift, averaged over 30 realizations, approaches the expected value for the image size in the case of uncorrelated trajectories. A similar behavior is observed in Figs. 3 and 4, which show the image size δ and the image shift θ as functions of the distance to the source. The image size is smaller than in the case of uncorrelated trajectories, while the image shift is significant.

This dependence of the image size and shift on the correlation length and distance to the source can be explained by the fact that the particles propagate through the same realization of the

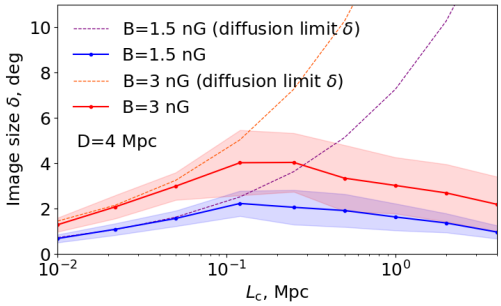

Figure 1: Angular size δ of the UHECR source image as a function of the IGMF correlation length for the realistic case where particles are emitted into the same realization of the IGMF (see Sec. 2.2 for details). Solid lines indicate the mean image size while the shaded regions indicate its standard deviation. Both the mean and standard deviation were calculated from 30 different IGMF realizations. For comparison, dashed lines show the analytical expectation for the case of uncorrelated trajectories, based on Eq. (7). The distance to the source was set to $D = 4$ Mpc.

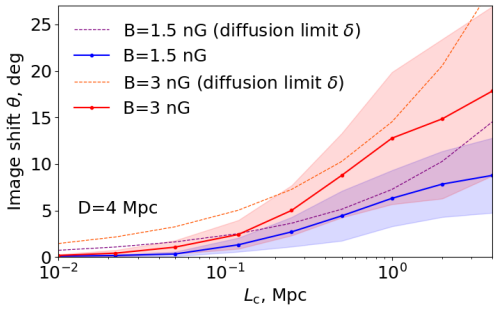

Figure 2: Same as Fig. 1, but here the solid lines and shaded regions represent the mean and standard deviation of the image shift θ. The dashed lines are the same as in Fig. 1 and show the analytical expectation of the image size δ for uncorrelated trajectories, based on Eq. (7).

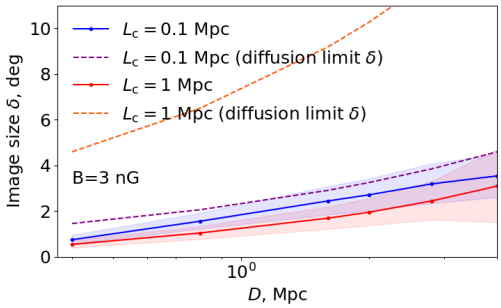

Figure 3: Angular size δ of the UHECR source image as a function of the distance to the source for the realistic case where particles are emitted into the same realization of the IGMF (see Sec. 2.2 for details). Different colors correspond to the different correlation lengths of the IGMF. The IGMF strength was fixed to $B = 3$ nG. As in Fig. 1, the solid lines and shaded regions represent the mean and standard deviation of the image sizes, while dashed line corresponds to Eq. (7).

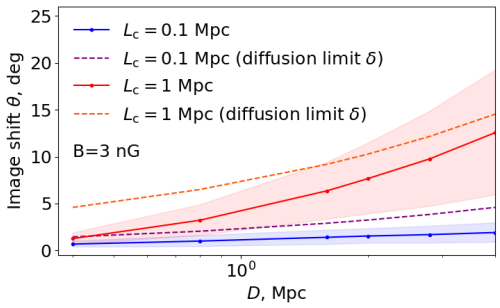

Figure 4: Same as Fig. 3 but here solid and dashed lines indicate the mean and standard deviation of the image shift θ.

PoS(ICRC2025)307

magnetic field. Close to the source, particles emitted in similar initial directions travel through almost the same magnetic field, causing the same deflection for all particles. This leads to a shift of the entire image while its size remains small. At the same time, the average shift angle follows the expected value of the image size. Only at a large distance, when particles pass through the ~ 100 magnetic domains and forget their initial conditions, the approximation of uncorrelated trajectories is restored.

2.3 Application to the Centaurus region excess

As a specific application of UHECR source image shifts induced by the IGMF, we consider the interpretation of the UHECR hotspot in the Centaurus region, observed at energies $E > 4 \cdot 10^{19}$ eV [10]. This is the most significant intermediate-scale anisotropy detected by the Auger.

A promising candidate source for this hotspot is the radio galaxy Cen A. However, in recent GMF models, the image of Cen A after deflections in the GMF is shifted relative to the position of the observed hotspot. For example in the `JF12` GMF model [11, 12], the image of Cen A is displaced by approximately 20° from the location of the observed excess. Similar shifts are observed when using more recent models such as `UF23` and `KST24`.

The image of Cen A, as observed at Earth, is shown in the left panel of Fig. 5. In the `JF12` model, the coherent GMF component shifts particles with rigidity of 10 EV (corresponding to carbon nuclei at energies $E \gtrsim 4 \cdot 10^{19}$ eV) by approximately 20° from the position of the excess toward the Galactic plane and lower Galactic longitudes. The turbulent component causes an additional angular spread around the image center. In contrast, the image of Cen A after passing throung both GMF and IGMF perfectly fits the position of the excess region as shown on the right panel of Fig. 5.

This alignment is achieved by selecting a particular IGMF realization in which the image of Cen A is first deflected toward the position of M83 and then further shifted by the GMF to match the location of the observed excess. Thus, the combined effect of IGMF and GMF still allows the Cen A to be the source of the excess.

3. Conclusions

The main result of the paper is that in the focusing mode, at a distance from the source less than one hundred magnetic field coherence lengths ($D < 100 \cdot L_c$), the standard expectation of diffusion theory, according to which UHECRs are isotropically distributed around their sources, is violated. Contrary to the predictions of diffusion theory, the observed images of UHECR sources are both smaller than expected and can be significantly displaced from the actual source positions, see Figs. 1 and 4.

Acknowledgments

We are grateful to Peter Tinyakov for useful discussions. The numerical modeling of the propagation of ultra-high-energy cosmic rays under the influence of large-scale cosmic magnetic fields (K.D.) is supported by the Russian Science Foundation grant 25-12-00111. The work of K.D. is supported by the Basis Foundation fellowship (grant No. 22-1-5-93-1). The work of D.S. is

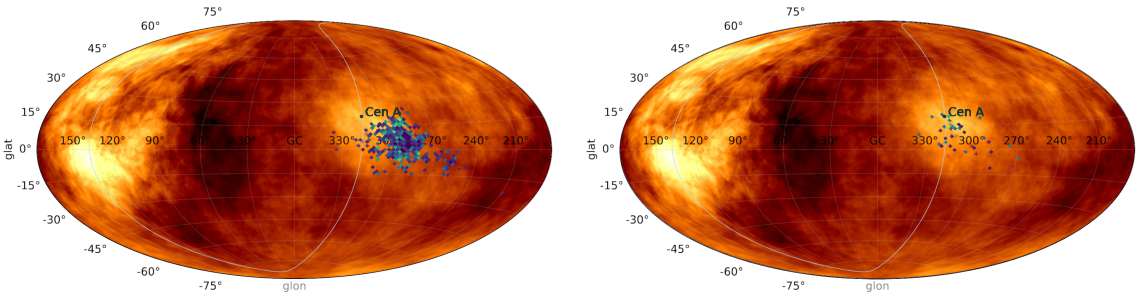

Figure 5: Arrival directions of particles with rigidity $R = 10$ EV emitted by the radio galaxy Cen A after propagation through the GMF and IGMF. In the left panel, the IGMF strength is set to zero. In the right panel, the IGMF strength is set to 3 nG and the correlation length $L_c = 0.3$ Mpc. The IGMF realization was selected to cancel out the deflections caused by the GMF.

supported by the French National Research Agency (ANR) grant ANR-24-CE31-4686. The work of A.K. is supported by the IISN project No. 4.4501.18.

References

[1] M. Unger and G.R. Farrar, *The Coherent Magnetic Field of the Milky Way*, *Astrophys. J.* **970** (2024) 95 [2311.12120].

[2] A. Korochkin, D. Semikoz and P. Tinyakov, *The coherent magnetic field of the Milky Way halo, the Local Bubble, and the Fan region*, *Astron. Astrophys.* **693** (2025) A284 [2407.02148].

[3] M.S. Pshirkov, P.G. Tinyakov and F.R. Urban, *New Limits on Extragalactic Magnetic Fields from Rotation Measures*, *Phys.Rev.Lett.* **116** (2016) 191302 [1504.06546].

[4] M.L. McCall, *A Council of Giants*, *Mon. Not. Roy. Astron. Soc.* **440** (2014) 405 [1403.3667].

[5] K. Dolgikh, A. Korochkin, G. Rubtsov, D. Semikoz and I. Tkachev, *Caustic-Like Structures in UHECR Flux after Propagation in Turbulent Intergalactic Magnetic Fields*, *J. Exp. Theor. Phys.* **136** (2023) 704 [2212.01494].

[6] K. Dolgikh, A. Korochkin, G. Rubtsov, D. Semikoz and I. Tkachev, *Images of the ultra-high energy cosmic rays from point sources*, *Advances in Space Research* **74** (2024) 5295.

[7] O. Kalashev, A. Korochkin, A. Neronov and D. Semikoz, *Modeling the propagation of very-high-energy γ-rays with the CRbeam code: Comparison with CRPropa and ELMAG codes*, *Astron. Astrophys.* **675** (2023) A132 [2201.03996].

[8] D. Harari, S. Mollerach, E. Roulet and F. Sanchez, *Lensing of ultrahigh-energy cosmic rays in turbulent magnetic fields*, *JHEP* **03** (2002) 045 [astro-ph/0202362].

[9] P.G. Tinyakov and I.I. Tkachev, *Deflections of cosmic rays in a random component of the Galactic magnetic field*, *Astroparticle Physics* **24** (2005) 32 [astro-ph/0411669].

[10] Pierre Auger collaboration, *An update on the arrival direction studies made with data from the Pierre Auger Observatory*, *PoS* **ICRC2023** (2023) 252.

[11] R. Jansson and G.R. Farrar, *A New Model of the Galactic Magnetic Field*, *Ap.J.* **757** (2012) 14 [1204.3662].

[12] R. Jansson and G.R. Farrar, *The Galactic Magnetic Field*, *Astrophys. J. Lett.* **761** (2012) L11 [1210.7820].